JACS
JOURNAL OF THE AMERICAN CHEMICAL SOCIETY

ARTICLE

pubs.acs.org/JACS

Glassy Nature of Water in an Ultraconfining Disordered Material: The Case of Calcium−Silicate−Hydrate

Mostafa Youssef,[†] Roland J.-M. Pellenq,[§,‡] and Bilge Yildiz*[,†]

[†]Department of Nuclear Science and Engineering and [‡]Department of Civil and Environmental Engineering, Massachusetts Institute of Technology, 77 Massachusetts Avenue, Cambridge, Massachusetts 02139, United States

[§]Centre Interdisciplinaire des Nanosciences de Marseille, CNRS and Marseille Université, Campus de Luminy, Marseille 13288, Cedex 09, France

Supporting Information

ABSTRACT: We present the structural and dynamic nature of water ultraconfined in the quasi-two-dimensional nanopores of the highly disordered calcium−silicate−hydrate (C-S-H), the major binding phase in cement. Our approach is based on classical molecular simulations. We demonstrate that the C-S-H nanopore space is hydrophilic, particularly because of the nonbridging oxygen atoms on the disordered silicate chains which serve as hydrogen-bond acceptor sites, directionally orienting the hydrogen atoms of the interfacial water molecules toward the calcium−silicate layers. The water in this interlayer space adopts a unique multirange structure: a distorted tetrahedral coordination at short range up to 2.7 Å, a disordered structure similar to that of dense fluids and supercooled phases at intermediate range up to 4.2 Å, and persisting spatial correlations through dipole−dipole interactions up to 10 Å. A three-stage dynamics governs the mean square displacement (MSD) of water molecules, with a clear cage stage characteristic of the dynamics in supercooled liquids and glasses, consistent with its intermediate-range structure identified here. At the intermediate time scales corresponding to the β-relaxation of glassy materials, coincident with the cage stage in MSD, the non-Gaussian parameter indicates a significant heterogeneity in the translational dynamics. This dynamic heterogeneity is induced primarily because of the heterogeneity in the distribution of hydrogen bond strengths. The strongly attractive interactions of water molecules with the calcium silicate walls serve to constrain their motion. Our findings have important implications on describing the cohesion and mechanical behavior of cement from its setting to its aging.

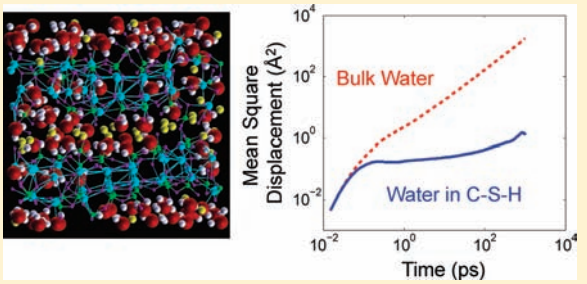

1. INTRODUCTION

Water is the most abundant compound on the surface of the Earth, and it is the principal constituent of all living organisms.[1] Very often water is found in confined geometries. Confined water at the nanometer scale differs significantly from bulk water. For example, by confining water in nanopores, so narrow that the liquid cannot freeze, it is possible to explore its properties well below its homogeneous nucleation temperature.[2,3] Widespread interest exists in the structure and dynamics of water in confinement and the influence of confinement on the hydrogen bonding, interfacial transport, and mechanics.[4,5] In the very fundamental biological system, the cell, water is confined between crowded bimolecular assemblies that are separated by 2−3 water layers.[6] Other systems of importance and to which water confinement is relevant are layered clays,[7−9] zeolites,[10,11] and cement.[12] In spite of this interest in understanding confined water properties, our knowledge in this area is still not fully developed. While there is sufficient evidence that the topology of and chemical effects from the confinement walls do influence the water structure and dynamics, the findings to date do not yet build a universally systematic picture. A representative example to the observed discrepancies is the viscosity of water confined between two hydrophilic surfaces. Major et al.[13] measured a viscosity that is 7 orders of magnitude greater for water under confinement than for bulk water. The confinement involved an interfacial separation less than 1 nm between two gold surfaces that were made hydrophilic by the chemisorption of a COOH-terminated alkanethiol self-assembled monolayer. On the other hand, Raviv et al.[14] observed a viscosity that is within only a factor of 3 of its bulk value when water was under confinement between mica surfaces with an interfacial separation ranging from 3.5 ± 1 to 0.4 nm or less. The dramatic increase in viscosity in the former was attributed to the hydrogen bonding of water molecules simultaneously to both hydrophilic surfaces, and the persistent fluidity in the latter was interpreted in terms of suppression of the formation of a highly directional hydrogen-bonded network. Both the observation and the interpretation of the water viscosity in these two hydrophilic confinement systems exemplify that, while the walls can prominently interfere with the hydrogen

Received: August 5, 2010
Published: February 4, 2011

bond network in the water, there are important open questions on the aspects of confinement geometry and chemical nature in explaining the confined water structure and properties.

There is also a set of consistent and important implications associated with the nature of confined water. In particular, these relate to the glassy state of the water confined by hydrophilic walls. Inelastic neutron scattering experiments showed that the structure of water in contact with the hydrophilic surfaces of Vycor glass nanopore walls at room temperature (298 K) is similar to that of bulk supercooled water at 273 K.[15] Later, Gallo et al.[16,17] showed by molecular dynamics (MD) simulations that water molecules residing close to the hydrophilic surface of Vycor glass behaved dynamically as if they were already below the mode coupling crossover temperature, with a slowing of the dynamics with respect to the bulk phase, although the simulation was performed at room temperature. Another important characteristic of the interfacial water at a hydrophilic surface was shown to be the increase of long-range spatial correlations compared to the bulk liquid water.[15,18] All these observations consistently suggest that the water confined by hydrophilic substrates, especially the water monolayer in direct interaction with the substrate, has a glassy nature. Nevertheless, the dynamics and the spatial characteristics of the structure of this glassy state have not yet been precisely described for a variety of confinement systems.

In this paper, we give our attention to a confined water system of both technological and scientific significance: the water confined in the interlayer space of a layered hydrated oxide called calcium−silicate−hydrate (C-S-H). This phase precipitates as clusters of nanoscale particles with an associated pore system as a result of mixing water and cement powder.[19−21] The pore system evolves during the cement setting process from a percolated macroporous to a microporous structure,[22] in which the smallest pores pose an ultraconfining environment for water between the layers of C-S-H. Cement cohesion,[23] transport of aggressive ions in cement paste,[24] and concrete creep and shrinkage mechanisms[25,26] are attributed to the chemistry of C-S-H particles as well as the water between and inside them. From the scientific perspective, C-S-H offers an interesting ultraconfinement environment where both the geometric and the chemical effects of the confinement on water can be probed. In a single-particle C-S-H system, water molecules are trapped mainly in the interlayer space between the highly disordered calcium−silicate layers, forming the so-called interlayer water. A smaller amount of them, constituting about 15% of the total water molecules in the C-S-H particle, are also trapped in small cavities within the layers, forming the intralayer water. Besides water, the interlayer space contains calcium ions that neutralize the negative charge of the calcium−silicate layers with a concentration of about three water molecules per calcium ion. This interlayer space has a thickness less than 1 nm and can be pictured as a highly concentrated ionic solution.[27] The calcium silicate layers in C-S-H have silicate chains that are defective compared to the uniform ones in the calcium−silicate layers of the crystalline analogue tobermorite. These defects are essentially the missing bridging silica tetrahedra. The existence of these defects provides sites that can serve for strong hydrogen bonding with water molecules and also enhances the connectivity within the interlayer space, increasing the possibility for water diffusion.[28] Such a connectivity does not exist in the interlayer space of tobermorite. The distortions and defects on the silicate chains in layered materials can have an even greater impact on the dynamics of the nanoconfined water than the actual pore size of the confinement, as shown by Ockwig et al.[29] using inelastic neutron scattering and molecular simulations. We will discuss the role of the defective silicate chains in our C-S-H system in the Results and Discussion section. For illustration purposes, Figure 1 depicts a recently reported molecular model of C-S-H[21] that was used in this paper. Further description of this C-S-H model is given in the Computational Approach section.

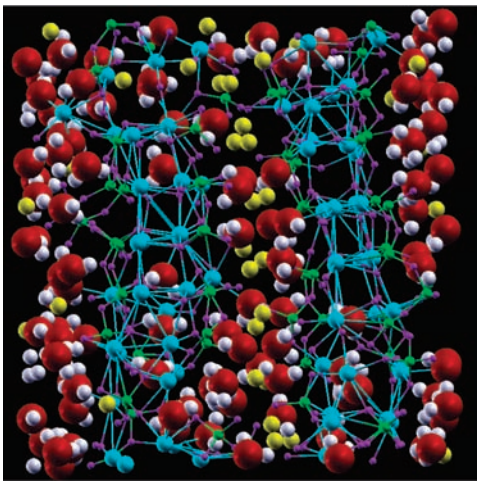

Figure 1. Molecular model of C-S-H that encompasses two highly disordered layers of calcium−silicate and water molecules trapped in the interlayer space together with the interlayer calcium ions. Few water molecules are trapped in small cavities in the calcium−silicate layers. White spheres are hydrogen atoms, red are water oxygen, purple are layer oxygen, green are silicon, light blue are layer calcium, and yellow are interlayer calcium. Water molecules are highlighted with a larger size compared to the other elements in the model.

Our objective is to provide a molecular-level description of the effect of the topologically and chemically heterogeneous nature of the C-S-H substrate on the properties of water that is quasi-two-dimensionally confined between the layers of this substrate. This is important not only for deciphering the nature of water in a realistic confined system but even more notably for informing the dependencies of the cement paste cohesion and mechanics on the microscopic structure and dynamics of the interfacial water.[18] This, in turn, provides directions for science-informed engineering of cementitious materials chemistry. In this study we considered the water confined in C-S-H particles rather than the water in the larger capillary pores that fills the space between the C-S-H particles in cement. The reason for this preference is twofold: (1) interfacial phenomena have the greatest effect on the structure and dynamics of the molecules that are directly associated with the interface walls,[30−33] and (2) starting from the very interfacially confined water and then scaling up to the inclusion of capillary pores would enable us to identify the role of water at each scale, from subnano- to macroscopic, in the cohesion and mechanical behavior of cement. The focus in this paper is on the static and dynamic description of the confined water. The results are explained in terms of structure, polarization, mobility, and dynamic heterogeneity of water molecules, tying them to the description of a multirange structure and glassy dynamics that arise in this system. The fact that our model explicitly and realistically[21] accounts for the structural disorder in C-S-H means that many of our results can be directly compared to experiments when they become available in the future. The

validation and discussion of our simulation results in this paper are done to a large extent on the basis of available experimental and theoretical descriptors from related systems in literature. The organization of the rest of this paper is as follows. In section 2, the model, force field, and simulation details are described. In section 3, numerical results are presented, accompanied by a discussion about their physical indications and significance. Finally, in section 4, we summarize our major observations and conclusions.

2. COMPUTATIONAL APPROACH

2.1. Molecular Model. Modeling a material composed of components with structural disorder is without a doubt a challenging problem. Recently,[21] a model that takes into account structural disorder for two calcium−silicate layers with the associated interlayer space was developed. As shown in Figure 1, the model consists of two sheets of calcium−silicates that entrap water molecules and interlayer calcium cations. The stoichiometric composition of the model is $(CaO)_{1.65}-(SiO_2)-(H_2O)_{1.73}$. The Cartesian coordinates of the atoms were provided in ref 21. With periodic boundary conditions in three dimensions, we approximate the C-S-H by infinite layers of disordered calcium−silicates that confine the quasi-two-dimensional sheets of water/interlayer calcium solution. This picture is relevant to understanding the building block of the cement paste. Our results here are derived from this infinite sheets of confined water system model, and not from the water in the capillary pores that surround the C-S-H particles in cement.

2.2. Force Field. We performed MD simulation using the recently developed CSHFF force field.[34] It is important to note here that many studies[30,35,36] emphasized the importance of including the flexibility and if possible also the polarizability in modeling water to describe the reactions at an interface or in ionic solutions. Famous rigid water models such as the extended simple point charge SPC/E,[37] while providing an excellent description of bulk water, are not able to represent solvation effects of dissolved ions and interfacial phenomena.[38] In our study, CSHFF includes a nonpolarizable but flexible version of SPC.[39] It will be evident in the Results and Discussion section that the flexibility is sufficient to qualitatively account for these effects with a considerably lower computational cost than having both flexibility and polarizability.

CSHFF has been developed recently for the family of calcium−silicate−hydrates. It uses optimized partial charges for the ions. It distinguishes between the "layer" calcium and "interlayer" calcium. It also treats the oxygen atoms that bridge two silica tetrahedra differently than the other layer oxygen atoms which do not serve a bridging role, which is important for the confinement problem here. Good agreement between the CSHFF results and Density Functional Theory predictions was shown for many structural and elastic properties of the minerals 11Å-Tobermorite and 14Å-Tobermorite.[34]

CSHFF is fast computationally, is very compatible with the C-S-H family, and has an excellent water potential that predicts a density of ∼1 g/cm^3 for bulk water at ambient conditions. The credentials of the water component of CSHFF are demonstrated in the Results and Discussion section. However, it does not achieve charge neutrality unless the partial charge of the nonbridging oxygen atoms is slightly modified. The charge modification is always less than 3% for all possible C-S-H phases. The parameters of the force field with the real-space cutoffs are given in the Supporting Information. Columbic interactions were computed using the Ewald summation method[40] with a precision of 1.0×10^{-8}.

2.3. Molecular Dynamics (MD). Finite temperature MD was used to study the equilibrium structure, polarization, and dynamical properties for both bulk and confined water. The code DL_POLY_2[41,42] was used to perform the simulation.

Bulk water was represented by 537 molecules in a cubic cell. C-S-H initial configuration was taken from ref 21 and doubled in the direction of the shortest cell vector to allow better sampling statistics for the equilibrium properties for confined water which is represented by 208 molecules. Isobaric−isothermal (NPT) simulations were performed for 1 ns with a target pressure and temperature of 0 atm and 300 K, respectively, to ensure that the system attains the equilibrium density. During these simulations, configurations with cell vectors close to the average equilibrium values were taken and used to start canonical ensemble (NVT) simulations. All systems were equilibrated again in the NVT ensemble for 250 ps, followed by two production runs. The first is 1 ns long with a time step of 0.1 fs to accurately sample the hydrogen bond dynamics, and the second is 5 ns long with a time step of 0.5 fs. Berendsen method was used to control both the pressure and the temperature, with a relaxation time of 0.5 ps for both the barostat and the thermostat. In all simulations, equations of motion were integrated using the Verlet−Leapfrog algorithm. Trajectories were recorded every 10 fs for the 1 ns run and every 50 fs for the 5 ns run.

3. RESULTS AND DISCUSSION

This section is presented in four subsections. First, we examine the nature of the interaction between the confined water and C-S-H in terms of hydrophilicity versus hydrophobicity. Second, we assess the structure of the confined water in C-S-H on a multirange basis and compare it to bulk water. Our comparison criteria are the doublet and triplet correlations. The triplet correlations reveal a similarity between the confined water structure and the structure of dense fluids and supercooled phases. This provides us with the evidence that the confined water can behave dynamically as a glassy material. In the third part, we examine and eventually demonstrate the glassy nature of the confined water dynamics in this quasi-two-dimensional hydrophilic system. Finally, we end this section by explaining this glassy behavior in terms of the heterogeneities in the hydrogen bond strengths in the interlayer space of C-S-H.

3.1. Hydrophilicity of the C-S-H Substrate. Characterizing the C-S-H substrate in terms of hydrophilicity and hydrophobicity provides the first step in understanding the nature of the interaction between the confined water and the calcium−silicate layers in the presence of interlayer calcium cations. To reveal this attribute, we examined the atomic density profile of oxygen (O_w) and hydrogen (H_w) of water in the direction normal to the plane of the calcium−silicate layers in addition to the distribution of the dipole moment of water molecules.

3.1.1. Atomic Density Profile. The atomic density profiles of O_w and H_w in water are shown in Figure 2. From the profiles in Figure 2, two pores of thicknesses that range from ∼6 to ∼9.5 Å are evident. The first pore extends from $z \approx 7.5$ to 13.5 Å, while the second extends from $z \approx 17.5$ to 23 Å and continues under periodic boundary conditions from $z \approx 0$ to 4 Å. The density in each pore is not the same, as expected for water in different micropores of such disordered materials.[9] The results presented here were averaged over both pores. Conclusions remain the same even if the properties of the confined water molecules are averaged over each single pore (see Supporting Information). The peaks that appear around $z \approx 5.5$ and 15 Å are due to water molecules trapped in small cavities in the calcium−silicate layers. The hydrogen density profiles show that water molecules point their hydrogen toward the calcium−silicate layers to form hydrogen bonds with the layer oxygen. This is the first signature of the hydrophilicity of the C-S-H layers.

The situation here is different than that in cationic clays, which are crystalline layered materials that have silicate chains grafted on the layers and cationic solution in the interlayer space. In cationic clays, the grafted, well-crystallized silicate chains are

dx.doi.org/10.1021/ja107003a |J. Am. Chem. Soc. 2011, 133, 2499–2510

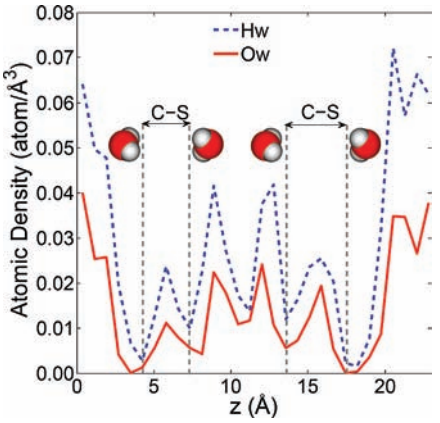

Figure 2. Atomic density profile of water hydrogen (H_w) and water oxygen (O_w) in the direction normal to calcium−silicate layers. C−S denotes the position of the calcium−silicate sheets, and the water molecules are schematically shown to align their hydrogen atoms toward the C−S layers.

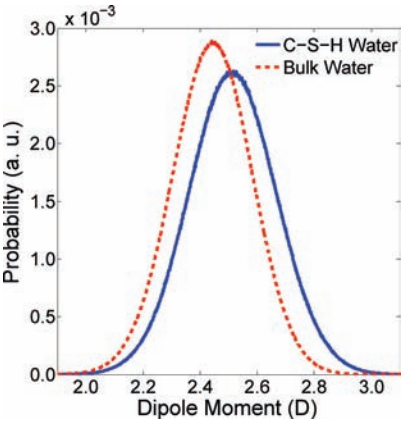

Figure 3. Distribution of the dipole moment of a single water molecule in bulk water and when confined in C-S-H. "a.u." denotes arbitrary units.

slightly hydrophobic.[43] The main reason for this is that most of the oxygen atoms in the silicate chains in a crystalline material occupy bridging sites and are not available to form hydrogen bonds with the interlayer water. On the other hand, in C-S-H, the disorder has a significant impact on its hydrophilicity. The finite length silicate chains, which are mainly dimers, allow a substantial amount of nonbridging oxygen atoms that provide acceptor sites for hydrogen bonds to the interlayer water, rendering this interface a hydrophilic one (see section 3.4).

3.1.2. Dipole Moment Distribution. Another metric we used to characterize the nature of the interaction between water and C-S-H is the distribution of the single water molecule dipole moment magnitude. The dipole magnitude distribution is sensitive to the environment in which water molecules exist, and an upshift of the dipole distribution would correspond to the hydrophilicity of the C-S-H confinement interface. We considered this distribution for the bulk and confined water, and the results are shown in Figure 3.

For the bulk liquid, the flexible SPC predicts an average dipole value of 2.44 D. The value of water dipole in the liquid state has been rarely reported experimentally. Badyal et al.[44] employed X-ray diffraction and deduced indirectly that the dipole moment of a liquid-state water molecule is 2.9 ± 0.6 D. From a modeling perspective, the value of a single water molecule dipole is very sensitive to the simulation details, as was shown by Puibasset and Pellenq[11] from Hartree−Fock *in vacuo* calculations and by Dyer and Cummings[45] using Car−Parrinello *ab initio* MD in the liquid state at 300 K. Given these uncertainties, we think that the predicted value for bulk water here is reasonably consistent with the range of results in prior reports. For confined water in C-S-H, we observe a positive shift to larger values of the dipole moment compared to that of bulk water. The shift is about 0.07 D (~2.9% of bulk value).

The upshift of the dipole magnitude distribution in C-S-H is another signature of the hydrophilicity of the C-S-H layer surface. For confined water in a hydrophilic framework, this upshift is due to the large electric field induced by the framework that polarizes the water molecules to an extent larger than the self-polarization in the normal liquid water.[46] For example, a similar upshift in the dipole distribution was observed in an MD simulation for water confined in a hydrophilic zeolite, using a fluctuating charge SPC water model.[47] In contrast, water confinement in a hydrophobic framework lowers the water dipole moment distribution compared to bulk.[11,46]

For layered materials with ionic solution in the interlayer space, there is a delicate balance between the nature of the layers and the identity of the ion in the interlayer space. This balance determines the domain in which these materials belong, hydrophilic versus hydrophobic.[43] For the C-S-H/water system we showed that the interaction is hydrophilic and pointed out that the disordered silicate chains play a role in biasing the system toward hydrophilicity. Added to this, the interlayer cation in C-S-H system, Ca^{2+}, works in the same direction (Supporting Information), enhancing the hydrophilic nature of C-S-H.

At this point, we also infer about the nature of the force field under consideration. Our results showed that the flexible and nonpolarizable SPC was sufficient to capture the confinement and ion solvation effects on the water molecule dipole qualitatively with a low computational cost. This supports the sufficiency of the flexibility in the water model to account for the confinement and solvation effects on water molecules in C-S-H.

3.2. Multirange Structure of Confined Water. Elucidating the structure of a confined fluid requires careful examination of the spatial correlations between the molecules. For a polar molecule such as water, considering both the site−site and dipole−dipole correlations is an asset. Typically the two-body site−site correlations, as epitomized in the partial radial distribution functions, are the most studied ones for liquids because of the possibility of direct comparison with neutron and X-ray scattering experiments. However, limiting the analysis to two-body correlations leaves considerable uncertainty in determining the geometrical structure. Extending the analysis to three-body correlations and even higher orders is tractable theoretically, but the lack of direct comparison with experiments limited such extension in the literature. We report here first the two- and three-body correlations to probe the short- and intermediate-range structure. These results show that the water confined in C-S-H adopts a unique multirange structure: a distorted tetrahedral coordination at short range up to 2.7 Å and a disordered structure similar to that of dense fluids and supercooled phases at intermediate range up to 4.2 Å. The dipole−dipole interactions, on the other hand, show that the spatial correlations persist up to 10 Å in this system, in spite of the disorder. In particular, the triplet correlations that we predict and present here can motivate experimental investigation of the same correlations in water confined in C-S-H, which are now possible through recent advances

dx.doi.org/10.1021/ja107003a |*J. Am. Chem. Soc.* 2011, 133, 2499–2510

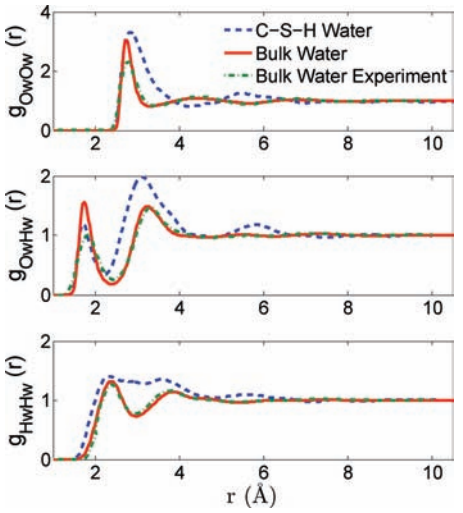

Figure 4. Simulated and experimental radial distribution functions for the bulk and confined water. Experimental results for bulk water were taken from ref 50.

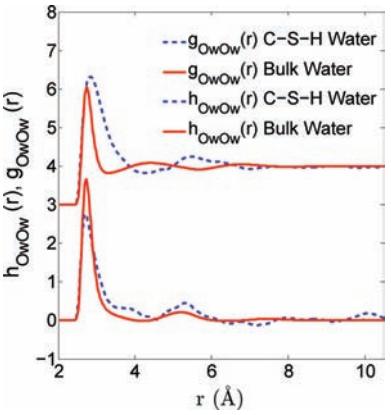

Figure 5. Oxygen−oxygen radial distribution function, $g_{O_wO_w}(r)$ (top), and dipole−dipole correlation function, $h_{O_wO_w}(r)$ (bottom), as a function of oxygen−oxygen distance r. The positive values of $h_{O_wO_w}(r)$ correspond to correlated dipole moment vectors, while negative values correspond to anticorrelated ones.

in X-ray absorption experiments[48] and inelastic neutron scattering experiments.[49]

3.2.1. Partial Radial Distribution Functions. We begin our analysis of the confined water structure by calculating the partial radial distribution functions, shown in Figure 4 for the oxygen−oxygen (O_wO_w), oxygen−hydrogen (O_wH_w), and hydrogen−hydrogen (H_wH_w) correlations. The peaks due to the intramolecular interactions have been omitted. In this figure, we compare the results obtained by the simulations for both the bulk and confined water with the experimentally determined data of these functions for bulk water taken from ref 50 by Soper. The differences in peak heights and minima depths between the bulk and confined water radial distribution functions determined by simulations are affected by the inaccuracy of the volume used in the normalization for the confined water in addition to the geometric and chemical effects of the confining walls. The bulk water completely fills the simulation cell volume, while the confined water occupies a fraction of the simulation cell, and it is difficult to quantify this fraction.[51] However, the differences in the positions and widths of the peaks and minima between the bulk and confined water radial distribution functions are only due to the chemistry and geometry of the confining environment and, thus, are more important to notice. Table 5 in the Supporting Information shows the position of the first peak, the position of the first minimum, and the coordination number in the first shell. It is evident that the water potential in CSHFF agrees reasonably well with the experiment in predicting the structure of bulk water.

These three correlation functions, for the confined water compared to bulk water, show clear signs of the distortion of the tetrahedral network of water when confined between the C-S-H layers. We summarize the significant traits that differ from the bulk water. CSHFF predicts that the oxygen−oxygen spatial correlations are extended to a larger distance, as indicated by the ∼0.9 Å shift of the first minimum and a shift in the second peak of ∼1 Å in $g_{O_wO_w}(r)$. This is accompanied by a larger coordination number in the first shell.

The major feature of the oxygen−hydrogen correlations is the reduction in the coordination number, which can be translated as a reduction in the number of hydrogen bonds (see section 3.4) among water molecules. This is the consequence of the available donor bonds of water molecules that are donated especially to the nonbridging oxygen atoms on the calcium−silicate layers. It is interesting also to note that the third peak is more pronounced than the third peak in bulk water. This shows that the site−site spatial correlations persist up to long distances for confined water.

The hydrogen−hydrogen radial distribution function for the confined water is very different than for bulk water. The first peak is broadened toward shorter distances, the first and second peaks merge together, and again the third peak becomes more pronounced compared to bulk.

The reasons for such deviation from the tetrahedral order in water are as follow: (1) the effect of the disordered hydrophilic calcium−silicate sheets that offer a significant number of acceptor sites for hydrogen bonds to the confined water, (2) the strong interlayer calcium solvation effects (Supporting Information), and (3) the quasi-two-dimensional confining geometry imposed by the substrate.

3.2.2. Dipole−Dipole Spatial Correlations. The permanent polarity of water molecules dictates strong orientational correlations through a dipole−dipole interaction. To assess the effect of confinement on these correlations, we computed the dipole−dipole correlation function for the bulk and confined water. This function is defined as[52]

$$h_{O_wO_w}(r) = 3g_{O_wO_w}(r)\langle\cos\theta\rangle \quad (1)$$

where θ is the angle between the dipole vectors of two water molecules at an oxygen−oxygen distance r. The results are shown in Figure 5, accompanied with $g_{O_wO_w}(r)$ for comparison.

Comparing $h_{O_wO_w}(r)$ and $g_{O_wO_w}(r)$ for bulk water shows that both functions continue to exhibit correlations up to 6 Å. The confinement extends the correlations in $h_{O_wO_w}(r)$ of water in C-S-H up to 10 Å. Cross-talk of water molecules from the separated pores of C-S-H does not interfere with these $h_{O_wO_w}(r)$ results, because we confirmed the similarly extended correlational behavior to be evident when the same calculations were performed by constraining the search only to the two-dimensional single pores of water isolated from each other in the model. Overall, these long-range dipole−dipole correlations demonstrate that the orientational correlations in the confined water in C-S-H persist considerably at longer distances than in bulk water.

dx.doi.org/10.1021/ja107003a |J. Am. Chem. Soc. 2011, 133, 2499–2510

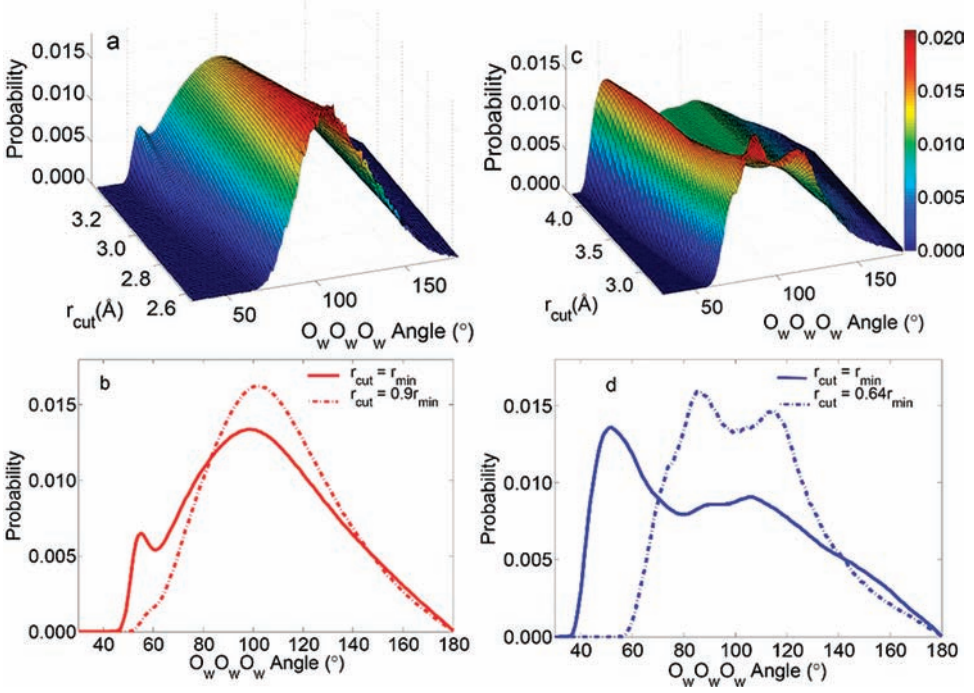

Figure 6. Distribution of the oxygen−oxygen−oxygen, $O_wO_wO_w$, angle between the oxygen atoms in three neighboring water molecules as a function of the angle and the search cutoff distance, r_{cut}: (a,b) bulk water and (c,d) confined water. In (a), the peak around 100° corresponds to the tetrahedral coordination around the central molecule, and the peak around 55° represents the presence of the interstitial molecule within the first coordination shell of the central molecule. In the 2D projection plots in (b,d), $r_{cut} = r_{min}$ corresponds to the usual cutoff distance, which is the first minimum in $g_{O_wO_w}(r)$, and $r_{cut} = fr_{min}$, $0 < f < 1$, was determined by searching for the distance below which the interstitial water molecule peak, ideally at 55°, disappears and only the tetrahedral-like coordination prevails.

We attribute the origin of these long-distance correlations to two possible mechanisms. First is the directional hydrogen bonding formed between the confined water molecules and the defective silicate chains that provides a substantial amount of acceptor sites through the nonbridging oxygen atoms. The role of such directional hydrogen bonding in enhancing the orientational correlations was similarly shown for the hydroxyl groups of sugar alcohols.[53] Second is the increase of the number of correlated molecules and spatial extent of the correlations as the temperature of a supercooled liquid decreases, approaching the glass transitions, recently demonstrated by Crauste-Thibierge.[54] We will show later in this paper that this confined water behaves in a glassy fashion similar to that of supercooled liquids as if it has an effective temperature lower than the actual temperature, enabling the persistence of long-range correlations. In fact, there might be synergistic interference between the two mechanisms that we propose here, since the observation made by Crauste-Thibierge et al.[54] was based on studying supercooled glycerol whose molecules were also hydrogen-bonded directionally by hydroxyl groups.

By combining the observations above from the two-body correlations, and prior to considering the three-body correlations, we reiterate that the local tetrahedral structure of water is distorted when confined in a disordered hydrophilic layered material such as C-S-H. However, some correlations, as evidenced in the dipole−dipole interactions, are enhanced and extend to longer distances for the confined water compared to bulk.

3.2.3. Triplet Correlations. Having examined the two-body correlations thoroughly, we turn our attention to the triplet correlations in order to depict more precisely the local structure of confined water. For this purpose, we report the oxygen−oxygen−oxygen ($O_wO_wO_w$) angular distribution among the neighboring water molecules. Experimentally for bulk water, this distribution is characterized by an intense and broad peak around 104° that corresponds to the tetrahedral coordination, and a smaller and sharp peak at 56°.[49] The peak at 56° is due to the angle between an interstitial water molecule in the first shell of a central molecule and a tetrahedral neighbor. To calculate this distribution, we choose a certain cutoff distance, r_{cut}, which defines two oxygen atoms as neighbors if they are separated by a distance less than this cutoff. The value of this cutoff distance is usually taken as the position of the first minimum, r_{min}, in the $g_{O_wO_w}(r)$ (see Figure 4). By setting the cutoff to r_{min} (Figure 6a, b), we found that the flexible SPC was able to reproduce these features accurately for bulk water. Furthermore, we searched for and identified the spatial extent below which the tetrahedral structure still prevails in both bulk and confined water. This was done by varying the cutoff between r_{min} and fractions of it as $r_{cut} = fr_{min}$, $0 < f < 1$, while calculating the $O_wO_wO_w$ angular distribution instead of calculating the distribution only at r_{min}. The result is shown by the 3D plots as a function of angle and r_{cut} in Figure 6a,c. For bulk water, we determined a critical cutoff value of $r_{cut} = 0.9r_{min} \approx 3.00$ Å, at which the interstitial water molecule peak disappears (see Figure 6b), and only the tetrahedral signature remains below $0.9r_{min}$. This indicates that the interstitial molecule site is in the outermost regions of the first hydration shell, more specifically between 3.00 and 3.33 Å.

Noteworthy characteristics arise in the $O_wO_wO_w$ distribution for water confined in the C-S-H. A significant enhancement of the interstitial molecule peak prevails at intermediate distances near r_{min} for water under confinement in C-S-H (Figure 6c) relative to that in bulk water (Figure 6a). This enhancement is the origin of the observed larger coordination number of water

dx.doi.org/10.1021/ja107003a |*J. Am. Chem. Soc.* 2011, 133, 2499–2510

molecules in the first shell of $g_{O_wO_w}(r)$ predicted by CSHFF (see Supporting Information, Table 5) for confined water. On the other hand, for confined water modeled using the CSHFF, the interstitial molecule peak remains until shorter distances into the first coordination shell, suggesting an increased jamming of the molecular arrangement. For the confined water, we also determined the critical cutoff below which a tetrahedral coordination, albeit distorted, prevails. This cutoff was found to be $r_{cut} = 0.64r_{min} \approx 2.72$ Å, which is shorter than that in bulk water. At and below this critical cutoff, we further observe two closely overlapping peaks, one centered near 90° and the other at 115° (Figure 6c,d). We suggest that these peaks arising at short distances belong to a distribution of distorted tetrahedral coordination because of the interference of the calcium−silicate layers and the interlayer calcium cations with the water hydrogen bond network. The peak around 90° is also a likely signature of the coordination of water molecules around the oxygen atoms of the silicate chains. To summarize, a distorted tetrahedral signature still governs the structure of confined water up to shorter distances (~2.72 Å) compared to that in bulk water (~3.00 Å). This piece of information was not available from our examination of the two-body correlations but became clear by a careful study of the $O_wO_wO_w$ angular distributions.

We now relate the identified $O_wO_wO_w$ angular distributions to those in dense and supercooled phases. Recently Strassle et al.[55] showed that bulk water at 670 K and 6.5 GPa exhibits an angular distribution similar to the one shown here for confined water by setting $r_{cut} = r_{min}$—similar in the sense that the tetrahedral peak weakens and the interstitial molecule peak gets enhanced. This distribution was also shown to be obeyed by a simple dense Lennard-Jones liquid[55] and by undercooled and liquid copper.[48] Such similarity in the triplet correlations between these dense phases and the confined water in C-S-H under consideration here gave us an enticing evidence that this confined water could behave dynamically in a glassy fashion. A direct link between structure and dynamics in supercooled phases was recently demonstrated,[56,57] and here we propose such a direct linkage between the structure and the dynamics of confined water. In section 3.3 we elaborate more on this aspect.

From the results presented in this section, we draw an overall picture of the structure of confined water in C-S-H with three major components at three length scales. First, at short distances, the tetrahedral coordination between water molecules is still intact, albeit distorted from its ideal coordination angles. Second, at intermediate scale (up to the distance of the first minimum in $g_{O_wO_w}(r)$), water molecules adopt a structure similar to that of dense fluids and supercooled phases. Finally, at large distances (up to 10 Å), dipole−dipole correlations remain significant. This, in turn, imposes a highly correlated orientational motion for the molecules.

As far as the structural properties that we considered in this section, we believe that CSHFF with its flexible SPC water potential predicts the confinement effects reliably. Our confidence is mainly built on its good performance in reproducing bulk water structural properties and the fact that the entire force field CSHFF is tailored for the family of C-S-H compounds.

3.3. Glassy Dynamics of Confined Water in C-S-H. As evidenced from the triplet correlations and the long-range dipole−dipole correlations in the previous section, the water confined in C-S-H exhibits structural characteristics similar to those in dense fluids and supercooled phases. It is also known that the glassy behavior of materials manifests itself more pronouncedly in the translational dynamics and is characterized by three stages, initiated by a ballistic motion at short time scales, followed by a cage behavior slowing the motion at intermediate scales, and finally a diffusive motion at long time scales.[58,59] To test our assertion about the glassy behavior of confined water in C-S-H, we investigated two universal characteristics that describe the slow dynamics of glassy materials: the MSD and the non-Gaussian behavior of the self-part of the van Hove function, which is attributed to the dynamical heterogeneity in the system.[60] While the MSD quantifies directly the translational dynamics, the non-Gaussian behavior allows us to probe and quantify the dynamical heterogeneity in our confined water system.[61]

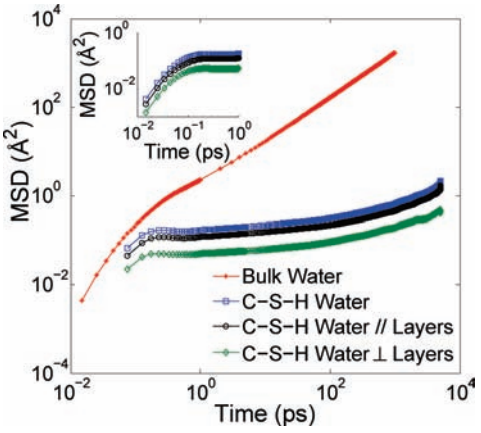

Figure 7. Mean square displacement (MSD) for the oxygen in bulk and confined water. The confined water results of the 5 ns simulation are in the main plot, while the inset shows the parabolic jump from the initial stages of the 1 ns simulation with the smaller time step.

3.3.1. Mean Square Displacement (MSD). Due to the quasi-two-dimensional geometry of the C-S-H ultraconfinement, we calculated not only the three-dimensional MSD but also the two-dimensional MSD parallel to the calcium−silicate sheets and the one-dimensional MSD perpendicular to those sheets. Utilizing the invariance under time translation, the MSD was calculated using

$$\langle \Delta \mathbf{r}^2(t) \rangle = \left\langle \frac{1}{N} \sum_{i=1}^{N} |\mathbf{r}_i(t+\tau) - \mathbf{r}_i(\tau)|^2 \right\rangle \qquad (2)$$

where $\mathbf{r}_i$ is the coordinate of the ith oxygen atom in water and the brackets denote averaging over multiple time origins, τ. The results of the calculations are plotted on a log−log scale in Figure 7. The MD simulation of the confined water was performed both for 1 ns with a 0.1 fs time step and for 5 ns using a longer time step of 0.5 fs to reveal all three stages of glassy dynamics.

For bulk water at $t < 0.4$ ps, there is an early stage parabolic jump followed by a linear behavior that is typical for liquids. For confined water in C-S-H, we observe the three stages of glassy dynamics. First, at short times, $t < 0.4$ ps, a ballistic motion prevails, with MSD proportional to t^2, since the motion of the water molecule is not yet affected by the presence of other molecules or atoms surrounding it. Second, between $t = 0.4$ ps and $t \approx 400$ ps for about three decades, all motion is slowed. This is because the water molecule is starting to collide with its neighboring molecules and atoms, thus only rattling in the cage

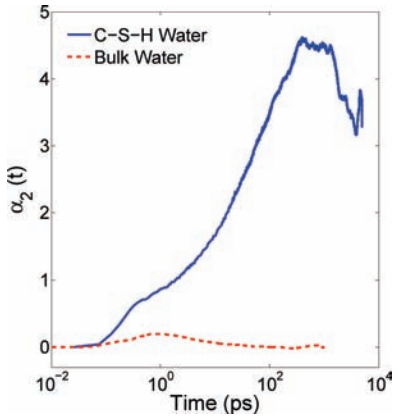

Figure 8. Non-Gaussian parameter $\alpha_2(t)$ calculated on the basis of the displacement of the oxygen atoms in bulk and confined water.

formed by the surrounding molecules. The water molecules participating in forming this cage are themselves in cages surrounding them. The molecules then succeed in escaping the cage and undergo diffusive motion, with MSD proportional to *t*. The transition from the cage regime to the diffusive regime is gradual, and there is no sharp transition time. Demonstration of these three stages of glassy dynamics supports our hypothesis that we deduced from the intermediate range structure of confined water described in section 3.2.3.

In addition to the glassy dynamics, the MSD shows that at early stages, the molecular displacement for water is almost isotropic in all directions. Later, when the diffusive motion is initiated, the value of the MSD parallel to the calcium−silicate layers (black circles) approaches the value of the three-dimensional MSD (blue squares) in Figure 7. This supports the quasi-two-dimensional character of the ultraconfinement environment of water between the calcium−silicate sheets. The two-dimensional diffusion is enhanced by the connectivity in the ultrathin interlayer space allowed by the defective silicate chains. Without this connectivity, the only motion available to water molecules would be the vibrations and restricted rotations, as in the case of the crystalline analogues of C-S-H.

3.3.2. Non-Gaussian Parameter. To further support the glassy dynamics evidenced above, we turn now to quantify the dynamical heterogeneity of the confined water, which was observed in many other dense two-dimensional glass-forming systems, both experimentally[62,63] and by simulation.[64] We use the deviation from the non-Gaussian behavior as a measure of the dynamic heterogeneity[61] in confined water in C-S-H. This is achieved by calculating a time-dependent non-Gaussian parameter (NGP) of the form[65,66]

$$\alpha_n(t) = \frac{\langle \Delta \mathbf{r}^{2n}(t) \rangle}{C_n \langle \Delta \mathbf{r}^2(t) \rangle^n} - 1,$$

$$C_n = 1 \times 3 \times 5 \times 7 \ \ldots (2n+1)/3^n \qquad (3)$$

for $n = 2, 3, 4, \ldots$. Time average is denoted by $\langle \cdots \rangle$, $\Delta \mathbf{r}^2(t)$ is the mean square displacement, and $\Delta \mathbf{r}^{2n}(t)$ is the mean $2n$ displacement. The non-Gaussian behavior is characterized by a non-vanishing $\alpha_n(t)$. For the purpose of our study, we utilized only $\alpha_2(t)$ as our NGP. The results of the calculated NGP for the oxygen atom of bulk and confined water are shown in Figure 8.

For the bulk liquid the result obtained is in agreement with what is known from prior simulations.[61] The NGP rises to a value of less than 0.2 on a time scale $t \approx 1$ps. It then drops again to zero on a time scale of few picoseconds. For the confined water the NGP exhibits features typical for supercooled liquids and glasses. It grows to a value of 4.5, which is an order of magnitude greater than the bulk case. The growth stops and a maximum is reached at about 400 ps, ending a stage known as β-relaxation. The large magnitude of the NGP in this time regime suggests that the translational dynamics of the confined water molecules is highly heterogeneous during the cage stage. The β-relaxation stage is followed by a slow drop of the NGP, starting another stage known as α-relaxation that corresponds to the onset of the diffusive motion. This transition from the β-relaxation to the α-relaxation stage is consistent with the transition from the cage to the diffusive regimes in our MSD results. In the hydrodynamic limit, $t \rightarrow \infty$, the NGP should decay to zero, reflecting the ergodicity of the system. It is very probable that the convergence of the NGP to zero cannot be captured in a reasonable simulation time using MD for the C-S-H system due to the time-scale limitations of the simulation method. Thus, we believe that exploring the longer time-scale evolution of the water confined in C-S-H requires a special treatment, for example by activation−relaxation based atomistic methods that can extend to longer time scales.[67−70]

We attribute the glassy dynamics similar to that of a supercooled liquid exhibited by the confined water in C-S-H at room temperature, particularly the cage effect in the MSD associated with the β-relaxation stage in the NGP, to two mechanisms. The first mechanism is the enhancement of the interstitial molecules in the first coordination shell, which forbids large displacements of water molecules. The local rearrangements could occur only through highly correlated motion of many particles in domains which are temporarily more fluidized than the background.[71,72] In the second mechanism this confined water behaves as if it is effectively at a lower temperature than the true temperature. The idea of "lower effective temperature" constraining the dynamics and forming a cage stage for water confined between the hydrophilic walls was suggested previously using neutron diffraction experiments.[73] Similarly, Gallo et al.[16] observed that water molecules residing close to the hydrophilic surface behaved as if they were already below the mode coupling crossover temperature when confined in a large (4 nm) nanopore, although the MD simulation was conducted at room temperature. Therefore, this dynamic constraint forming a cage stage in the MSD of water ultraconfined in C-S-H at room temperature is imposed because of the attractive interactions and stronger hydrogen bonds of water molecules with the calcium−silicate hydrophilic walls. We believe that this second mechanism is the dominant one in determining the heterogeneous glassy dynamics of this confined water. This is supported by the fact that in bulk supercooled water, the cage effect is a consequence of the increase of the hydrogen bond stiffness, which makes the cage rigid,[17] rather than a density increase associated with the increase in the interstitial molecule peak. Moreover, all possible interpretations for the behavior of the supercooled water were shown[74] to be governed by the strength of the directionality and the cooperativity of the hydrogen bonds. To prove this assertion for the water in the C-S-H ultraconfining environment, next we assess the distribution of hydrogen bond strengths in this system.

3.4. Hydrogen Bonding in C-S-H. In this section, we discuss the glassy heterogeneous dynamics on the basis of the heterogeneities in the hydrogen bond strengths of the confined water molecules in C-S-H. First, we present our criteria in defining the

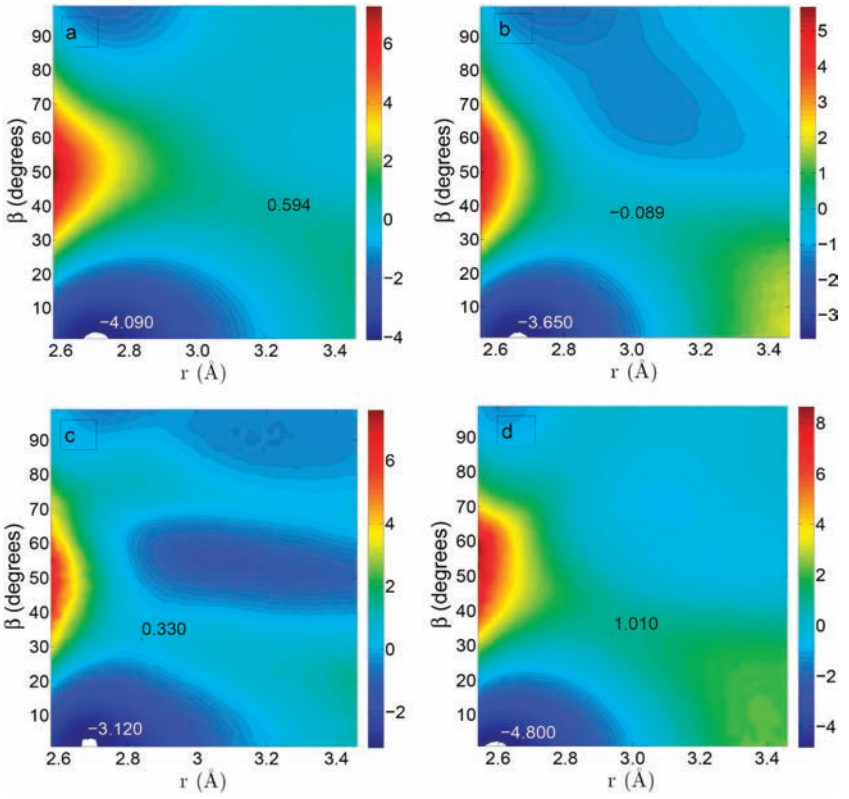

Figure 9. Potential of mean force based on the $r-\beta$ pair calculated from molecular dynamics simulation using CSHFF force field: (a) water/water hydrogen bond in bulk water, (b) water/water hydrogen bond in C-S-H, (c) water/bridging oxygen in C-S-H, and (d) water/nonbridging oxygen in C-S-H. In all cases the global minimum is marked by a white dot, and the saddle point is marked by a black cross. The contours in the color bar are in units of kT.

hydrogen bonds in this system. We then quantify the number of hydrogen bonds in both bulk and confined water on the basis of our criteria. We demonstrate that water molecules are hydrogen-bonded not only to each other but also to the silicate chains in C-S-H, as was suggested by the mass density profile (Figure 2). Finally, using the hydrogen bond time correlation function, we rank the identified types of hydrogen bonds according to their bond strengths. This picture proves that there is a distribution of hydrogen bond strengths of water molecules in the system, the stronger ones being the ones between water molecules and the nonbridging oxygen atoms on the disordered silicate chains.

3.4.1. Hydrogen Bond Definition. It is common to define the hydrogen bond between a donor and an acceptor on the basis of energetic and/or geometric criteria. One of the most used geometric criteria is that of Luzar and Chandler,[75,76] in which a donor and acceptor are defined to be hydrogen-bonded if the distance between the two oxygen atoms (r) is less than 3.5 Å and the angle (β) between the O−H ray in the donor and the O−O ray is less than 30°. While this criterion describes the hydrogen bonds that form in bulk water very well, we believe that there is a variety of situations in which this criterion may not apply accurately. Examples for such situations are the hydrogen bonds among confined water molecules, between interfacial water and a hydrophilic surface,and between water molecules in concentrated ionic solutions.[77,78] In fact, our C-S-H system encompasses all these possibilities. In order to reduce the arbitrariness in defining the hydrogen bond, we adopt the systematic approach developed by Kumar et al.[79] in generating the hydrogen bond criteria from two-dimensional (2-D) potentials of mean forces (PMF). This approach not only renders the hydrogen bond definition less arbitrary but also is insightful. Kumar et al. discussed the construction of the 2-D PMFs for four different choices of angles and distances. In each PMF, there is a low-energy basin located at short distances that corresponds to the hydrogen-bonded states. This lowest energy basin is separated by a saddle point from another higher-energy basin that corresponds to the non-hydrogen-bonded states. The equipotential contour that goes through the saddle point defines the cutoff for the hydrogen bond. Here we consider the $r-\beta$ PMF.

Kumar et al.'s construction of the $r-\beta$ PMF, which we adopted here, is as follows: $g(r,\beta)$ is defined as the ratio of the average number of oxygen atoms[80] that are separated by a distance between r and $r+\mathrm{d}r$ and simultaneously form an OOH angle (the OH ray in the donor) between β and $\beta+\mathrm{d}\beta$ to the same average if the atoms were non-interacting. The PMF, $W(r,\beta)$, is then

$$W(r,\beta) = -kT \ln g(r,\beta) \qquad (4)$$

where k is the Boltzmann constant and T is the temperature. We calculated the PMF for bulk water and for three types of hydrogen bonds in C-S-H: the hydrogen bonds among the confined water molecules, the hydrogen bond donated by a water molecule and accepted by a bridging oxygen atom on the silicate chains, and finally the hydrogen bond donated by a confined water molecule and accepted by a nonbridging oxygen atom on the silicate chains. In Figure 9 we show these cases calculated from the 1 ns MD simulation. The two basins

dx.doi.org/10.1021/ja107003a |*J. Am. Chem. Soc.* 2011, 133, 2499–2510

Table 1. Average Number of Hydrogen Bonds $\langle n \rangle$ Per Water Molecule (O_w), Per Bridging Oxygen (O_B), and Per Nonbridging Oxygen (O_{NB})

donor −acceptor	$\langle n_{donated} \rangle$	$\langle n_{accepted} \rangle$
O_w-O_w (bulk)	1.80	1.80
O_w-O_w (C-S-H)	0.55	0.55
O_w-O_B (C-S-H)	0.12	0.38
O_w-O_{NB} (C-S-H)	1.12	0.63

discussed above are obvious on each PMF. Both the saddle point and the global minimum are marked with their values on each PMF contour plot.

3.4.2. Average Number of Hydrogen Bonds. The criteria developed above were used to determine the average number of hydrogen bonds per water molecule and per oxygen atom on the calcium−silicate sheets. The results are summarized in Table 1.

The average total number of hydrogen bonds in which a water molecule participates in bulk is 1.8 + 1.8 = 3.6. On the other hand, the confined water molecule in C-S-H participates, on average, in 2.34 hydrogen bonds. The bonds of confined water in C-S-H are counted as follows: For a water molecule, on the average 0.55 are donated to other water molecules, another 0.55 are accepted from the other molecules, 0.12 are donated to the bridging oxygen atoms (O_B) on the silicate chains, and finally 1.12 are donated to the nonbridging oxygen (O_{NB}) on the silicate chains. It should be noted that the confined water does not accept any bonds from the oxygen atoms on the silicate chains, since the latter are not hydroxylated. Therefore, the total is 0.55 + 0.55 + 0.12 + 1.12 = 2.34 (see also the Supporting Information). The confined water molecules in C-S-H participate in fewer hydrogen bonds than the bulk water molecules (2.34 vs 3.6); 53% of the bonds in which the confined water molecule participates are donated to the calcium−silicate layers. Furthermore, the nonbridging oxygen accepts significantly more hydrogen bonds from the confined water compared to the bridging oxygen (0.63 vs 0.38).

3.4.3. Ranking of Hydrogen Bond Strengths. To distinguish the heterogeneity of the hydrogen bond strengths in this confinement system, we calculated the history-independent hydrogen bond time correlation function from the following definition:[75,81,82]

$$C(t) = \frac{\langle \delta h(t) \delta h(0) \rangle}{\langle \delta h(0) \delta h(0) \rangle} \quad (5)$$

where $\delta h(t) = h(t) - \langle h \rangle$, $h(t)$ is a binary operator between a donor and acceptor that takes a value of one if the pair is bonded and zero if not, and $\langle h \rangle$ is the average of the operator over all pairs and times. The time correlation functions for the four types of hydrogen bonds listed in Table 1 are plotted in Figure 10.

For $t \leq 0.1$ ps the correlation functions show a fast decay due to the fast librational motion. During this period, the bulk water (O_w-O_w bulk) hydrogen bond correlation function relaxes slower than both O_w-O_B and O_w-O_w in CSH. This is expected, as it is known that confinement blue-shifts the frequency of the librational modes of water.[29,83] What is surprising is that the relaxation of O_w-O_{NB} remains slower than for bulk water even at these short time scales, which indicates the high strength of this category of hydrogen bonds. For $t \geq 0.1$ ps the bulk water hydrogen bond correlation function decays rapidly, while the

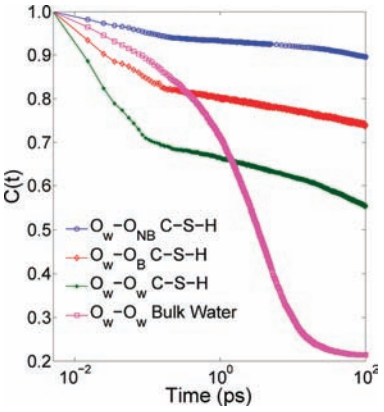

Figure 10. Hydrogen bond time correlation function for the four types considered here. The notation used in the legend is as follows: water molecule, O_w; bridging oxygen, O_B; and nonbridging oxygen, O_{NB}.

three hydrogen bonds in CSH exhibit plateaus typical of supercooled water.[84] Thus, we rank the hydrogen bonds from the strongest to the weakest as follows:

1 O_w-O_{NB}, water/nonbridging oxygen in C-S-H;
2 O_w-O_B, water/bridging oxygen in C-S-H;
3 O_w-O_w, water/water in C-S-H;
4 O_w-O_w, water/water in bulk liquid water.

We also note that the silicate chains are topologically disordered, and this disorder can further induce a wide distribution of bond strengths within the two top categories of bonds above. We suggest that these distributions of the hydrogen bond strengths in the interlayer space of C−H are the major drivers for the dynamical heterogeneity in the β-relaxation stage (Figures 7 and 8). The stiffness of these bonds, in particular that of the O_w-O_{NB} bonds under confinement, imposes a rigid cage stage in the translational dynamics for the water molecules.[85]

4. CONCLUSION

Controlling the macroscopic mechanical and chemical properties of a wide class of materials of important applications, such as zeolites, clays, and cement, requires a fundamental understanding of the nature of water confined at the nanoscale pores of these materials. In this paper, we studied by means of molecular simulations the water confined in the quasi-two-dimensional pores of width less than 1 nm in calcium−silicate−hydrate, which is the major binding phase in cement. Our results indicated that a well-parametrized flexible water potential such as that in CSHFF is adequate to capture the confinement and ion solvation effects in a computationally efficient way.

Both the interlayer calcium and the defective silicate chains in C-S-H render a hydrophilic interaction between the confined water and C-S-H. The defective silicate chains offer acceptor hydrogen-bonding sites to the confined water molecules mainly through the nonbridging oxygen atoms on the silicate layers. The interlayer calcium, as a divalent cation, facilitates the sorption of the water molecules in the interlayer space, enhancing the hydrophilicity in the interface region. The overall hydrophilic nature of this confining interface increases the polarity of the water confined at this interface.

The confined water in C-S-H adopts a multicharacteristic structure. Each characteristic of the structure manifests itself on a distinct length scale. At short distances up to 2.7 Å, the

tetrahedral coordination of water molecules is still preserved, albeit distorted from the ideal tetrahedral coordination angle. At an intermediate range up to 4.2 Å, the triplet correlations of the oxygen−oxygen−oxygen angle distributions demonstrated that the confined water adopts a structure similar to that of dense fluids and supercooled phases. At larger distances up to 10 Å, orientational correlations persist through directional hydrogen bonds to the substrate, as evidenced through the dipole−dipole interactions between water molecules.

The intermediate range structure provided us with evidence that the confined water can behave dynamically as a glassy material. By examining the mean square displacement and the non-Gaussian parameter, we showed that the water ultraconfined by the hydrophilic interfaces of C-S-H exhibits a three-stage dynamics, with a clear cage stage of highly heterogeneous dynamics, characteristic of glassy phases. We showed that this heterogeneous glassy dynamics is induced because of the heterogeneity in the distribution of hydrogen bond strengths, including the strong hydrogen bonding between water molecules and the nonbridging oxygen on the calcium−silicate hydrophilic walls, serving to constrain the motion of water molecules at the interface. The reasoning for this behavior as analyzed in the C-S-H system is transferable to other hydrophilic confining environments which are heterogeneous topologically and chemically. Our findings on the microscopic nature of water suggest that nontrivial properties of water can arise in this C-S-H confinement environment, and these properties should be treated explicitly in assessing the cohesion and mechanics of cement from its formation to its end of life.

■ ASSOCIATED CONTENT

Supporting Information. Force field parameters; additional notes about the structure of confined water, the effect of interlayer calcium, and the counting of hydrogen bonds; and a 2.2 ns molecular dynamics simulation movie in AVI format that exemplifies the heterogeneity in the dynamics of water molecules. In the movie, a confined water molecule in C-S-H is tagged in cyan. The molecule breaks its surrounding cage by a hopping motion. Color code in the movie is the same as in Figure 1 except that all calcium cations are yellow. This material is available free of charge via the Internet at http://pubs.acs.org.

■ AUTHOR INFORMATION

Corresponding Author
byildiz@mit.edu

■ ACKNOWLEDGMENT

We thank S. Yip and J. Grossman for stimulating and helpful discussions. Funding for this work was provided by the Center for Advanced Nuclear Energy Systems (CANES) at MIT and by the Concrete Sustainability Hub (CSH) at MIT.

■ REFERENCES

(1) Eisenberg, D.; Kauzmann, W. *The Structure and Properties of Water*; Oxford University Press: New York, 1969.
(2) Chen, S.-H.; Mallamace, F.; Mou, C.-Y.; Broccio, M.; Corsaro, C.; Faraone, A; Liu, L. *Proc. Natl. Acad. Sci. U.S.A.* **2006**, *103*, 12974.
(3) Bergman, R.; Swenson, J. *Nature* **2000**, *403*, 283.
(4) Kete, S.; Xu, Z.; Ihle, B.; Buehler, M. J. *Nat. Mater.* **2010**, *9*, 359.
(5) Hu, M.; Goicochea, J. V.; Michel, B.; Poulikakos, D. *Nano Lett.* **2010**, *10*, 279.
(6) Mentre, P. *Cell. Mol. Biol.* **2001**, *47*, 709.
(7) Karaborni, S.; Smit, B.; Heidug, W.; Urai, J.; van Oort, E. *Science* **1996**, *271*, 1102.
(8) Marry, V.; Rotenberg, B.; Turq, P. *Phys. Chem. Chem. Phys.* **2008**, *10*, 4802.
(9) Creton, B.; Bougeard, D.; Smirnov, K. S.; Guilment, J.; Poncelet, O. *Phys. Chem. Chem. Phys.* **2008**, *10*, 4879.
(10) Cailliez, F.; Trzpit, M.; Soulard, M.; Demachy, I.; Boutin, A.; Patarin, J.; Fuchs, A. H. *Phys. Chem. Chem. Phys.* **2008**, *10*, 4817.
(11) Puibasset, J.; Pellenq, R. *J. Phys. Chem. B* **2008**, *112*, 6390.
(12) Bordallo, H.; Aldridge, L.; Desmedt, A. *J. Phys. Chem. B* **2006**, *110*, 17966.
(13) Major, R.; Houston, J.; McGrath, M.; Siepmann, J.; Zhu, X.-Y. *Phys. Rev. Lett.* **2006**, *96*, 177803.
(14) Raviv, U.; Laurat, P.; Klein, J. *Nature* **2001**, *413*, 51.
(15) Bellissent-Funel, M.-C. *J. Mol. Liq.* **1998**, *78*, 19.
(16) Gallo, P.; Rovere, M.; Spohr, E. *Phys. Rev. Lett.* **2000**, *85*, 4317.
(17) Gallo, P.; Rovere, M.; Spohr, E. *J. Chem. Phys.* **2000**, *113*, 11324.
(18) Lombardo, T. G.; Giovambattista, N.; Debenedetti, P. G. *Faraday Discuss.* **2009**, *141*, 359.
(19) Taylor, H. F. W. *Cement Chemistry*, 2nd ed.; Thomas Telford: London, 1997.
(20) Allen, A.; Thomas, J.; Jennings, H. *Nat. Mater.* **2007**, *6*, 311.
(21) Pellenq, R.; Kushima, A.; Shahsavari, R.; Van Vliet, K.; Buehler, M.; Yip, S.; Ulm, F.-J. *Proc. Natl. Acad. Sci. U.S.A.* **2009**, *106*, 16102.
(22) Ridi, F.; Luciani, P.; Fartini, E.; Baglioni, P. *J. Phys. Chem. B* **2009**, *113*, 3080.
(23) Jönsson, B.; Wennerström; Nonat, A.; Cabane, B. *Langmuir* **2004**, *20*, 6702.
(24) Mindess, S.; Young, J. F. *Concrete*; Prentice Hall: Englewood Cliffs, NJ, 1981.
(25) Vandamme, M.; Ulm, F.-J. *Proc. Natl. Acad. Sci. U.S.A.* **2009**, *106*, 10552.
(26) Neville, A. M. *Properties of Concrete*, 4th ed.; Prentice Hall: Upper Saddle River, NJ, 1995.
(27) Sposito, G.; Prost, R. *Chem. Rev.* **1982**, *82*, 553.
(28) Churakov, S. V. *Am. Mineral.* **2009**, *94*, 156.
(29) Ockwig, N. W.; Greathouse, J. A.; Durkin, J. S.; Cygan, R. T.; Daemen, L. L.; Nenoff, T. M. *J. Am. Chem. Soc.* **2009**, *131*, 8155.
(30) Cicero, G.; Grossman, J.; Schwegler, E.; Gygi, F.; Galli, G. *J. Am. Chem. Soc.* **2008**, *130*, 1871.
(31) Dokter, A. M.; Woutersen, S.; Bakker, H. J. *Proc. Natl. Acad. Sci. U.S.A.* **2006**, *103*, 15355.
(32) Baruah, B.; Roden, J. M.; Sedgwick, M.; Correa, M.; Crans, D. C.; Levinger, N. E. *J. Am. Chem. Soc.* **2006**, *128*, 12758.
(33) Cicero, G.; Grossman, J. C.; Catellani, A.; Galli, G. *J. Am. Chem. Soc.* **2005**, *127*, 6830.
(34) Shahsavari, R.; Pellenq, R.; Ulm, F.-J. *Phys. Chem. Chem. Phys.* 2011, *13*, 1002–1011.
(35) van Maaren, P.; van der Spoel, D. *J. Phys. Chem. B* **2001**, *105*, 2618.
(36) Smirnov, K.; Bougeard, D. *Chem. Phys.* **2003**, *292*, 53.
(37) Berendsen, H.; Grigera, J.; Straatsma, T. *J. Phys. Chem.* **1987**, *91*, 6269.
(38) van Buuren, A.; Marrink, S.; Berendsen, H. *J. Phys. Chem.* **1993**, *97*, 9206.
(39) Teleman, O.; Jonsson, B.; Engstrom, S. *Mol. Phys.* **1987**, *60*, 193.
(40) Allen, M.; Tildesley, D. *Computer Simulation of Liquids*; Oxford University Press: New York, 1987.
(41) Smith, W.; Yong, C.; Rodger, P. *Mol. Simul.* **2002**, *28*, 385.
(42) Smith, W. *Mol. Simul.* **2006**, *32*, 933.
(43) Greenwell, H. C.; Jones, W.; Coveney, P. V.; Stackhouse, S. *J. Mater. Chem.* **2006**, *16*, 708.
(44) Badyal, Y. S.; Saboungi, M. -L.; Price, D. L.; Shastri, S. D.; Haeffner, D. R.; Soper, A. K. *J. Chem. Phys.* **2000**, *112*, 9206.

(45) Dyer, P. J.; Cummings, P. T. *J. Chem. Phys.* **2006**, *125*, 144519.
(46) Coudert, F.-X.; Vuilleumier, R.; Boutin, A. *ChemPhysChem* **2006**, *7*, 2464.
(47) Shirono, K.; Daiguji, H. *Chem. Phys. Lett.* **2006**, *417*, 251.
(48) Di Cicco, A; Trapananti, A; Faggioni, S. *Phys. Rev. Lett.* **2003**, *91*, 135505.
(49) Ricci, M. A.; Bruni, F.; Giuliani, A. *Faraday Discuss.* **2009**, *141*, 347.
(50) Soper, A. K. *J. Phys.: Condens: Matter* **2007**, *19*, 335206.
(51) Park, S.-H.; Sposito, G. *J. Phys. Chem. B* **2000**, *104*, 4642.
(52) Nymand, T. M.; Linse, P. *J. Chem. Phys.* **2000**, *112*, 6386.
(53) Nakanishi, M.; Nozaki, R. *Phys. Rev. E* **2010**, *81*, 041501.
(54) Crauste-Thibierge, C.; Brun, C.; Ladieu, F.; L'Hote, D.; Biroli, G.; Bouchaud, J.-P. *Phys. Rev. Lett.* **2010**, *104*, 165703.
(55) Strassle, T.; Saitta, A. M.; Godec, Y. L.; Hamel, G.; Klotz, S.; Loveday, J. S.; Nelmes, R. J. *Phys. Rev. Lett.* **2006**, *96*, 067801.
(56) Mosayebi, M.; Del Gado, E.; Ilg, P.; Ottinger, H. C. *Phys. Rev. Lett.* **2010**, *104*, 205704.
(57) Xu, L.; Mallamace, F.; Yan, Z.; Starr, F. W.; Buldyrev, S. V.; Stanley, H. E. *Nature Phys.* **2009**, *5*, 565.
(58) Kob, W. *J. Phys.: Condens. Matter* **1999**, *11*, R85.
(59) Roder, A.; Kob, W.; Binder, K. *J. Chem. Phys.* **2001**, *114*, 7602.
(60) Chaudhuri, P.; Berthier, L.; Kob, W. *Phys. Rev. Lett.* **2007**, *99*, 060604.
(61) Caprion, D.; Matsui, J.; Schober, H. R. *Phys. Rev. Lett.* **2000**, *85*, 4293.
(62) Kagel, W. K.; van Blaaderen, A. *Science* **2000**, *287*, 290.
(63) Weeks, E. R.; Crocker, J C.; Levitt, A. C.; Chobfield, A.; Weitz, D. A. *Science* **2000**, *287*, 627.
(64) Hurley, M. M.; Harrowell, P. *J. Chem. Phys.* **1996**, *105*, 10521.
(65) Rahman, A. *Phys. Rev.* **1964**, *136*, A405.
(66) Boon, J. P.; Yip, S. *Molecular Hydrodynamics*; Dover: New York, 1991.
(67) Kushima, A.; Lin, X.; Li, J.; Eapen, J.; Mauro, J. C.; Qian, X.; Diep, P.; Yip, S. *J. Chem. Phys.* **2009**, *130*, 224504.
(68) Kushima, A.; Lin, X.; Li, J.; Eapen, J.; Mauro, J. C.; Qian, X.; Diep, P.; Yip, S. *J. Chem. Phys.* **2009**, *131*, 164505.
(69) Lau, T. T.; Kushima, A.; Yip, S. *Phys. Rev. Lett.* **2010**, *104*, 175501.
(70) Fan, Y.; Kushima, A.; Yildiz, B. *Phys. Rev. B* **2010**, *81*, 104102.
(71) Adam, G.; Gibbs, J. H. *J. Chem. Phys.* **1965**, *43*, 139.
(72) Zangi, R.; Rice, S. A. *Phys. Rev. E* **2003**, *68*, 061508.
(73) Dore, J. In *Correlations and connectivity*; Stanley, E. H., Ostrowsky, N., Eds.; Kulwer Academic: Dordrecht, 1990.
(74) Stokely, K.; Mazza, M. G.; Stanley, H. E.; Franzese, G. *Proc. Natl. Acad. Sci. U.S.A.* **2010**, *107*, 1301.
(75) Luzar, A.; Chandler, D. *Nature* **1996**, *379*, 55.
(76) Luzar, A.; Chandler, D. *Phys. Rev. Lett.* **1996**, *76*, 928.
(77) Hammerich, A. D.; Buch, V.; Mohamed, F. *Chem. Phys. Lett.* **2008**, *460*, 423.
(78) Hammerich, A. D.; Buch, V. *J. Chem. Phys.* **2008**, *128*, 111101.
(79) Kumar, R.; Schmidt, J. R.; Skinner, J. L. *J. Chem. Phys.* **2007**, *126*, 204107.
(80) The oxygen atom can be in a water molecule, in a hydroxyl group, or on an oxide surface.
(81) Chowdhary, J.; Landanyi, B. M. *J. Phys. Chem. B* **2009**, *113*, 4045.
(82) Stillinger, F. H. *Adv. Chem. Phys.* **1975**, *31*, 1.
(83) We confirmed this through calculating the vibrational density of states, which is not shown here.
(84) Starr, F. W.; Nielsen, J. K.; Stanely, H. E. *Phys. Rev. E* **2000**, *62*, 579.
(85) The movie in the Supporting Information shows a tagged molecule that translates through a hopping mechanism. The hopping is restricted by strong hydrogen bonding to the calcium−silicate sheets. Once the bond is broken, the molecule hops and gets trapped again in another hydrogen bond.